Chapter 1

Numerical Analysis of the Liquid-Gas-Solid Three Phase Flow Inside AWJ Nozzle

Xinping Long and Qi Liu

Additional information is available at the end of the chapter

http://dx.doi.org/10.5772/intechopen.75938

Abstract

The multiphase flows inside the two abrasive waterjet (AWJ) nozzles with different abrasive inlet tube angles are simulated using the standard k-ε turbulence model based on the Euler-Lagrangian approach. The volume of fluid (VOF) method is employed to simulate the water-air multiphase flows. And, the abrasive particles are treated as dilute dispersed phase and tracked with the discrete particle method (DPM). The results indicate that the abrasive inlet tube angle has little impact on the water-phase flows. Further analysis shows that a larger abrasive inlet tube angle can enhance the particle accelerations. The particle number independence analysis is conducted, and the results indicate that sufficient particles should be tracked in order to obtain statistically representative results. The effects of particle initial velocities, particle shape factors, and the restitution coefficients on the predicted particle movements are further analyzed for the two nozzles with abrasive inlet tube angles of 45° and 60°. The results reveal that at the current velocity range, the particle initial velocities have little impact on the predicted particle velocities. However, both the shape factors and the restitution coefficients play an important role on the calculated particle velocities. The results provide a deeper understanding of particle acceleration performance inside the AWJ nozzles with different abrasive inlet tube angles.

Keywords: abrasive waterjet, multiphase flow, DPM, VOF

1. Introduction

The abrasive waterjet (AWJ) is originally developed to improve the cutting ability of the pure waterjet (PWJ). As a new type of cold cutting technology, the AWJ is performed to cut target materials with water-containing abrasive particles at high pressures. Generally, the AWJ is capable of cutting or manufacturing both brittle and ductile materials without imposing thermal

impact on the target materials. It also has the advantages of high machining versatility, small machining force, and high flexibility compared with other manufacturing methods. Therefore, the AWJ has been widely applied in numerous fields [1–4]. Recently, the potential of the AWJ technology for high precision cutting or manufacturing of hard-to-machine materials has made the AWJ again receive much attention [5, 6].

It should be mentioned that the AWJ is different from the abrasive slurry jet (ASJ). And, the definition of the two types is mainly based on the mixing process of abrasive particles with fluid. For the ASJ, in the high-pressure tank, the abrasive particles are premixed with water to produce the so-called slurry which is directly ejected from the nozzle. However, for the AWJ, as illustrated in **Figure 1**, the high-pressure pure water is firstly ejected from the orifice into the mixing chamber where the abrasive particles and the air are simultaneously entrained to mix with the high-speed water, and then the AWJ is generated in the focus tube. Therefore, there are only two phases of flows (particle and water) in ASJ nozzle but three phases of flows (particle, water, and air) in AWJ nozzle. The operating pressure of AWJ is much higher than that of the ASJ, and the energy utilization of AWJ is comparatively lower. Thus, extensive efforts have already been made to investigate the cutting, machining, and energy transfer efficiency of the so-called AWJ technology [7, 8]. Momber investigated the energy transfer during the high-speed waterjet formation process and also the abrasive particle mixing and

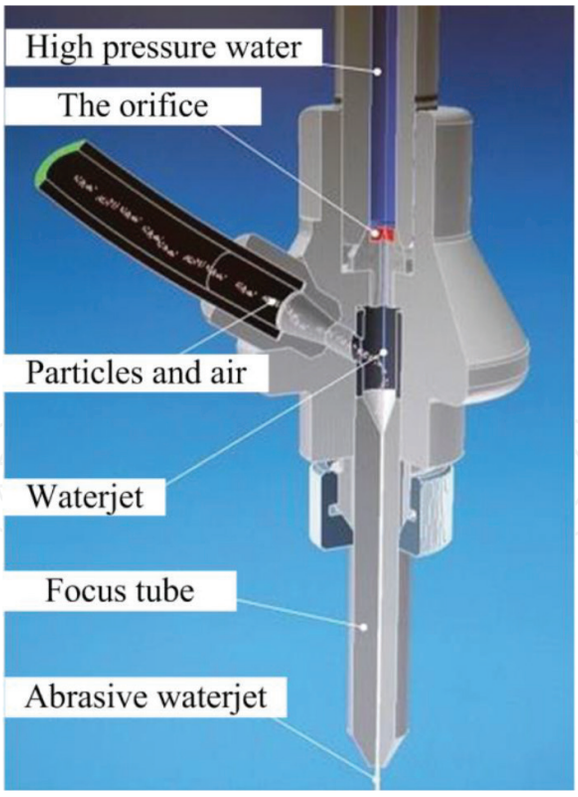

Figure 1. The AWJ cutting system and AWJ nozzle [6].

http://dx.doi.org/10.5772/intechopen.75938

acceleration processes by conducting impact-force measurements [7]. Lee et al. studied the material removal mechanisms of AWJ with micro-sized abrasive particles [9]. Shanmugam and Masood experimentally investigated the effects of AWJ operating parameters on the kerf taper angle of two types of layered composites [10]. Coray et al. tested a 5:1 scale AWJ equipment models to study the kinetic energy distributions of the abrasive particles together with the jet structure. They reported that due to the strong interactions among the three phases the signal differences between water phase and abrasive particles could not yet be distinguished experimentally [11].

It is already well known that the AWJ nozzle, as an important component of the AWJ equipment, has a significant impact on the overall manufacturing performances and is crucial for improving machining quality and reducing energy consumption. Thus, a better understanding of the effects of nozzle parameters on the jet structure and abrasive particle movements is essential to develop high-performance AWJ equipment. However, due to the small dimensions of the AWJ nozzle and the highly aggressiveness of abrasive particles, conducting experiments to study the three phases of flows inside the AWJ nozzle is still very challenging. And, the accurate measurement of the complex multiphase flows which involves ultrahigh-speed water, air, and abrasive particles inside the extremely small nozzle space may even impossible at present. With the rapid development of computational fluid dynamics (CFD) and computing ability, numerical simulations of this complex internal flows have been made possible, which provides an effective way to gain a better understanding of the multiphase interaction mechanisms. Long et al. conducted numerical simulations to investigate the particle movement inside the AWJ nozzle using different particle shape factors. The results revealed that a smaller particle shape factor could enhance the overall particle acceleration process [6]. Yang et al. numerically studied the abrasive particle motions and the corresponding erosion rate inside the AWJ nozzle at the pressures beyond 300 MPa. It was revealed that the proposed numerical model provided a reliable way to investigate the AWJ nozzle internal multiphase flows [12]. Basha et al. simulated the internal multiphase flows inside an AWJ nozzle and investigated the jet flow dynamic characteristics. It was confirmed that the numerical simulations could accurately capture the AWJ nozzle performance [13].

Despite the abovementioned efforts, the complex interactions between the fluid phases and the particles inside the AWJ nozzle are not yet fully understood, and the effects of numerical model parameters on the simulation results are not well investigated. Also, the effects of nozzle structure on the multiphase flows are not well studied. Inspired by the mentioned work, the present paper is devoted to investigating the liquid-gas-solid multiphase flows in AWJ nozzles with different abrasive inlet tube angles at a given high operating pressure under different model parameters based on three-dimensional Euler-Lagrangian numerical simulations. The effects of particle initial velocities, particle shape factors, and particle-wall restitution coefficients on the predicted particle velocities are discussed. The effects of abrasive inlet tube angles on the multiphase flows are further analyzed. The results can help to provide guidance for future CFD-aided AWJ nozzle optimization.

2. Governing equations and numerical method

As illustrated in **Figure 1**, the high-pressure water is firstly ejected from the orifice, and the resulted high-speed water jet then enters into the mixing chamber. By the high-speed jet entraining effects, the air phase together with the abrasive particles is entrained into the mixing chamber where strong interactions are expected. The abrasive particles are mixed and accelerated by the high-speed fluid phase and finally ejected through the long focus tube to impact on the workpiece. The present study is performed by simulating the steady-state multiphase flows in AWJ nozzles based on the time-averaged Navier-Stokes equations. It was reported that the volume fractions of the abrasive particles in the AWJ nozzle was normally less than 10% [14]. Thus, the Euler-Lagrangian method is finally utilized for all the present simulations. Both the water phase and the air phase are treated as continuums and are computed in Eulerian reference frame using the finite volume method. However, the abrasive particles are considered as discrete phase and are solved in Lagrangian reference frame using the discrete particle method (DPM).

2.1. Governing equations for continuous phases

The water-air multiphase flows are modeled using the volume of fluid (VOF) model. The volume fraction-based composition of AWJ is approximately 0.2–0.5% abrasive particles, 4–6% water phase, and 93–95% air phase [15]. The air phase is finally chosen as the primary phase in the present simulations, and thus the continuity equation for the volume fraction of the water phase can be written as

$$\frac{\partial(\alpha_w u_i)}{\partial x_i} = 0 \tag{1}$$

where α_w is the volume fraction of water and u_i is velocity. The volume fraction of the primary phase α_a can be directly obtained by the simple equation:

$$\alpha_a = 1.0 - \alpha_w \tag{2}$$

As the VOF is based upon the single fluid assumption, the air phase and the water phase share the same velocity field, and a single momentum equation is solved throughout the computational domain. Therefore, the governing equation for the conservation of momentum can be given as

$$\frac{\partial(\rho u_i u_j)}{\partial x_j} = -\frac{\partial p}{\partial x_i} + \frac{\partial}{\partial x_j}\left[(\mu + \mu_t)\left(\frac{\partial u_i}{\partial x_j} + \frac{\partial u_j}{\partial x_i} - \frac{2}{3}\frac{\partial u_k}{\partial u_k}\delta_{ij}\right)\right] \tag{3}$$

where u_i and u_j are the velocities in the x_i and x_j coordinate directions, respectively. p and ρ stand for the pressure and the mixture density. μ is the laminar viscosity of the fluid mixture.

It should be noted that the one-way coupling method is applied indicating that the particle movement is influenced by the continuous phase, but the flow phase is not influenced by the particle motion. So, there are no additional source terms in Eq. (3).

The fluid mixture properties of water and air in Eq. (3) are calculated as

$$\begin{aligned} \mu &= \alpha_a \cdot \mu_a + \alpha_w \cdot \mu_w \\ \rho &= \alpha_a \cdot \rho_a + \alpha_w \cdot \rho_w \end{aligned} \tag{4}$$

where subscripts *a* and *w* represent air and water, respectively.

To predict the turbulent viscosity μ_t, the standard *k*-ε turbulence model is used. The transport equations of turbulence kinetic energy *k* and the turbulence dissipation rate ε can be given as

$$\frac{\partial(\rho k)}{\partial t} + \frac{\partial\left(\rho k u_j\right)}{\partial u_j} = \frac{\partial}{\partial x_j}\left[\left(\mu + \frac{\mu_t}{\sigma_k}\right)\frac{\partial k}{\partial x_j}\right] + P_t - \rho\varepsilon \tag{5}$$

$$\frac{\partial(\rho\varepsilon)}{\partial t} + \frac{\partial(\rho\varepsilon\, u_j)}{\partial u_j} = \frac{\partial}{\partial x_j}\left[\left(\mu + \frac{\mu_t}{\sigma_\varepsilon}\right)\frac{\partial \varepsilon}{\partial x_j}\right] + C_{\varepsilon 1} P_t \frac{\varepsilon}{k} - C_{\varepsilon 2}\rho\frac{\varepsilon^2}{k} \tag{6}$$

where μ_t is computed by $\mu_t = C_\mu \rho k^2/\varepsilon$ with $C_\mu = 0.09$, σ_k and σ_ε are the turbulent Prandtl number for *k* and ε, and their values are set as 1.3 and 1.0, respectively. The other two empirical constants are given as $C_{\varepsilon 1} = 1.44$ and $C_{\varepsilon 2} = 1.92$.

2.2. Disperse-phase tracking method

The interactions among the particles are neglected as the volume-based concentration of abrasive particles in the present cases is less than 10%. The so-called one-way coupling method is adopted to track the abrasive particles. As the diameters of the particles are small, the rotation motions of the abrasive particles are neglected. The forces acting on each particle include the drag force, the virtual mass force, and the pressure gradient force. The governing equation for each abrasive particle in the Cartesian coordinate form can be given as

$$\frac{du_p}{dt} = F_d(u - u_p) + F_{vm} + F_p \tag{7}$$

where u_p is the particle velocity and F_d is the drag force per unit particle mass, which can be calculated as

$$F_d = \frac{18\mu}{\rho_p d_p^2}\frac{C_D Re_p}{24} \tag{8}$$

where Re_p stands for the particle Reynolds number which defined as

$$Re_{\mathrm{p}} = \frac{\rho\, d_{\mathrm{p}} |u - u_p|}{\mu} \tag{9}$$

where d_{p} represents the particle diameter and ρ_p stands for the particle density. The drag coefficient C_{D} is predicted by the following equation [16]:

$$C_{\mathrm{D}} = \frac{24}{Re_{\mathrm{p}}}\left(1 + b_1 Re_{\mathrm{p}}^{\,b_2}\right) + \frac{b_3 Re_{\mathrm{p}}}{b_4 + Re_{\mathrm{p}}} \tag{10}$$

where

$$\begin{cases} b_1 = \exp\left(2.3288 - 6.4581\varphi + 2.4486\,\varphi^2\right) \\ b_2 = 0.0964 + 0.5565\varphi \\ b_3 = \exp\left(4.905 - 13.8944\varphi + 18.4222\,\varphi^2 - 10.2599\,\varphi^3\right) \\ b_4 = \exp\left(1.4681 + 12.2584\varphi - 20.7322\,\varphi^2 + \mathrm{T}\ 15.8855\,\varphi^3\right) \end{cases} \tag{11}$$

where φ is termed as the shape factor to take the particle sphericity into consideration as shown in **Figure 2**. According to its definition, $\varphi = s/S$, where s represents the nominal surface area of a sphere particle which has the same volume as the real particle and S is the actual surface area of the particle; $\varphi = 1$ indicates that the particle is spherical, where φ is smaller than unity indicating that the particle is nonspherical. A smaller value of the shape factor represents an increase of the particle irregularity.

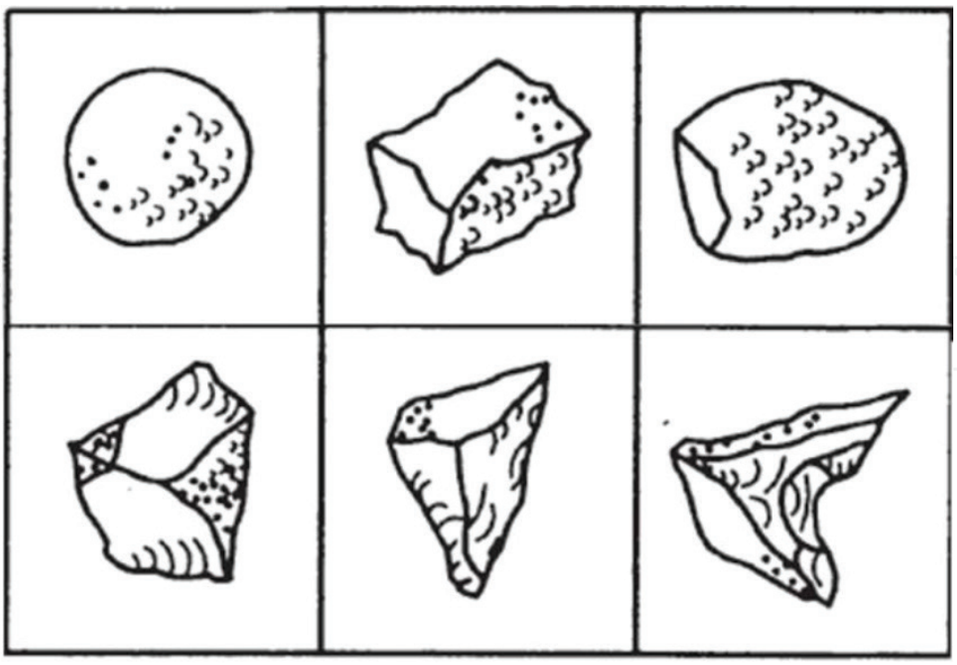

Figure 2. Typical shapes of abrasive particle [17].

The virtual mass force acting on each abrasive particle can be calculated as

$$F_{\mathrm{vm}} = \frac{1}{2}\frac{\rho}{\rho_{\mathrm{p}}}\frac{d}{dt}(u - u_{\mathrm{p}}) \tag{12}$$

The effect of virtual mass is significant when the particle density ρ_{p} is much smaller than the fluid phase density ρ.

The pressure gradient force is caused by a pressure difference and can be modeled as

$$F_{\mathrm{p}} = \frac{\rho}{\rho_{\mathrm{p}}}\nabla p \tag{13}$$

The diameters of abrasive particles used in the present simulations are very small, and the pressure difference over one particle diameter distance can be ignored. Therefore, only the drag force is taken into consideration in the current study.

For turbulent flows, the fluid velocity can be divided into the mean velocity and the random fluctuation velocity. To predict the effect of turbulent flow velocity fluctuations on the particle movement, the random walk model (RWM) is used. The turbulent fluctuating velocity is modeled as

$$u' = \varsigma\sqrt{\frac{2k}{3}} \tag{14}$$

where k is the calculated turbulence kinetic energy and ζ is a Gaussian distributed random number.

A reflecting boundary condition is adopted to consider the interactions between the abrasive particles and the wall boundaries. The particles reach the wall and change directions after the collisions. Two famous parameters, namely, the normal restitution coefficient e_{n} and the tangential coefficient e_{τ}, are defined as follows:

$$\begin{aligned} e_n &= \frac{v_{p2}}{v_{p1}} \\ e_\tau &= \frac{u_{p2}}{u_{p1}} \end{aligned} \tag{15}$$

where v_{p} is the particle velocity normal to the wall and the corresponding subscript 1 and 2 represent before and after the collision, respectively. Likely, the tangential coefficient accounts for the momentum changes in the direction tangential to the wall boundary. The restitution coefficients for both directions equal to unity indicate a fully elastic collision which means that there is no energy loss during the collision.

2.3. Computational model and numerical setup

A typical geometry of the three-dimensional AWJ nozzle is illustrated in **Figure 3**. The high-pressure water tube diameter is 4 mm, the orifice diameter is 0.4 mm, the mixing chamber

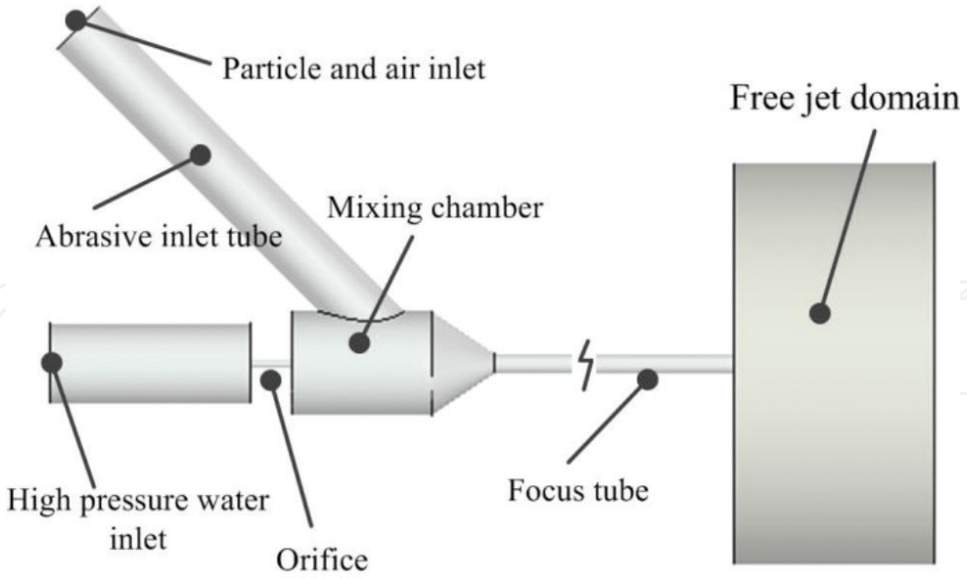

Figure 3. Geometry of the AWJ nozzle for the 3D simulation.

diameter is 5 mm, and the abrasive particle inlet tube diameter is 3 mm. The focus tube has a diameter of 1 mm with the length of 60 mm. Two AWJ nozzles with different abrasive inlet tube angles are modeled in the present study as illustrated in **Figure 4**. Model 1 represents the AWJ nozzle with the abrasive inlet tube angle of 45°, and model 2 stands for the AWJ nozzle with the abrasive inlet tube angle of 60°. The computational domains of the two models are meshed as shown in **Figures 5** and **6**. In order to ensure the accurate tracking of VOF surface, a mesh refinement is conducted around the orifice and the water-air interface regions. Both tetrahedral and hexahedral meshes are generated inside the computational domains, and high-density mesh regions are located where large gradients are expected. The grid independence analysis for both the two models indicate that the results predicted with the meshes with about 900,000 nodes will not change with further refinement of mesh resolution. The meshes used in the subsequent simulations are given in **Figures 5** and **6**.

The pressure inlet boundary condition with a given pressure of 300 MPa is specified at the water inlet, while atmospheric pressure is fixed at the air inlet boundary. At the free jet domain boundary region, the outlet boundary condition is applied with a pressure fixed at

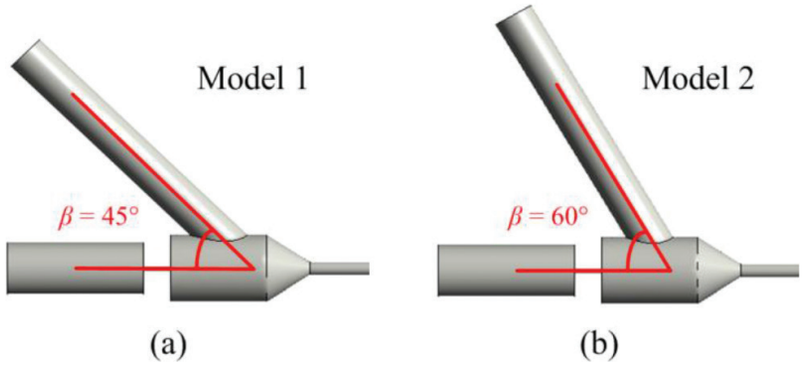

Figure 4. AWJ nozzles with different abrasive inlet tube angles.

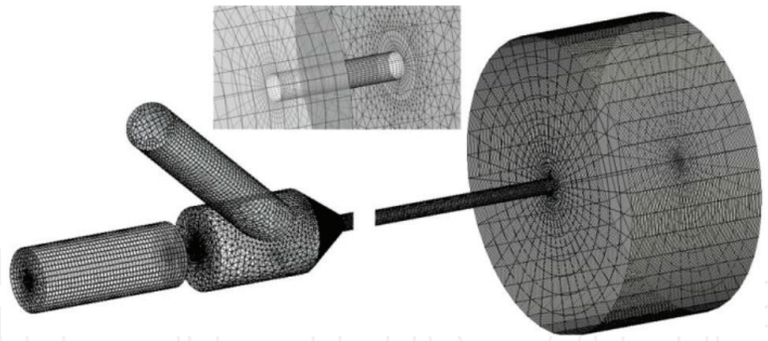

Figure 5. Computational mesh used in the simulations (model 1).

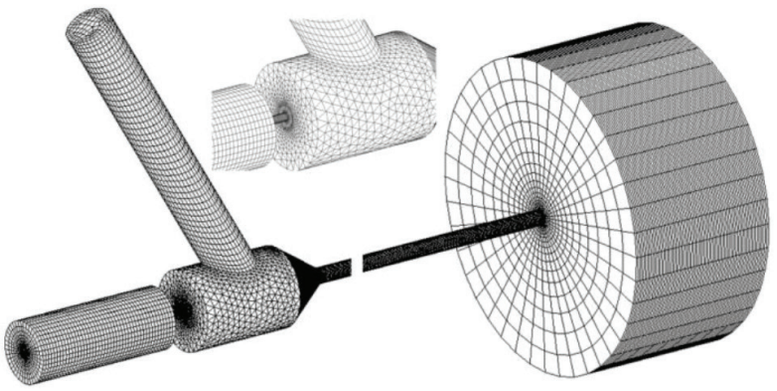

Figure 6. Computational mesh used in the simulations (model 2).

the atmospheric pressure. The no-slip wall boundary condition is specified at the walls. The abrasive particles are injected into the computational domains with uniform velocity with a given mass flow rate of 5 g/s. And, the density of abrasive particle is 2600 kg/m^3. The interactions between the wall and particles are modeled by specifying the restitution coefficients. The abovementioned steady-state governing equations for air and water phases are finally discretized in space domain using the finite volume method (FVM) with SIMPLE algorithm. The QUICK scheme is used to approximate the phase volume fraction. The second-order accurate central differential scheme is adopted to discretize the diffusion terms. And, the second-order accurate upwind scheme is implemented to discretize the other convective terms. The convergence criterions for all the cases are specified as that the residuals for each equation drop below 10^{-4}. Once the steady-state simulations of continuous phases are completed, the abrasive particles are released, and the particle trajectories are correspondingly predicted. All the simulations are performed with commercial software Ansys Fluent 15.0.

3. Results and discussion

3.1. Flow field inside AWJ nozzle

Figure 7 shows the predicted flow patterns inside the two AWJ nozzles at the same operating pressure of 300 MPa. The typical free jet structures are captured by the present model in the

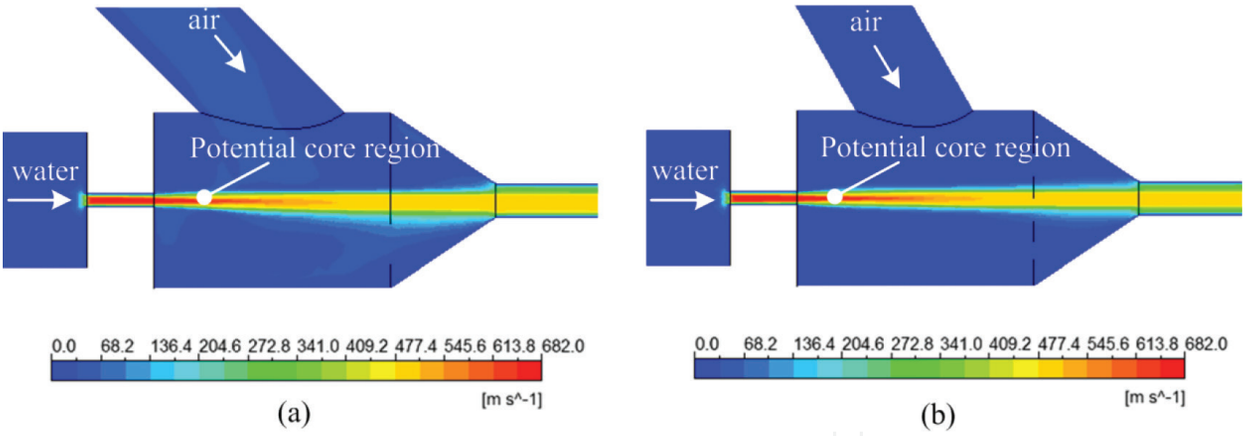

Figure 7. Velocity contour inside (**a**) model 1 and (**b**) model 2 AWJ nozzles.

mixing chamber. It can be seen that the high-pressure water ejected from the orifice produces a high-speed water jet. The predicted potential core region has the maximum velocity, and the axial velocity begins to decay significantly further downstream. Due to the high-speed region in the chamber, a comparatively low-pressure region is generated, and thus the air is entrained into the nozzle by the water jet entraining effect. The predicted area-weighted average velocity at the air inlet is about 37 m/s. It is noted that the comparatively low-velocity region in the velocity is slightly asymmetric, which is mainly caused by the presence of the particle inlet tube. The velocity distributions in the axial lines of the two types of nozzles are shown in **Figure 8**. There is a small gap between the velocity profiles in the mixing chamber. However, the two lines are almost collapsed together in the focus tubes. Generally, the impact of abrasive inlet tube angle on the fluid flow is not significant.

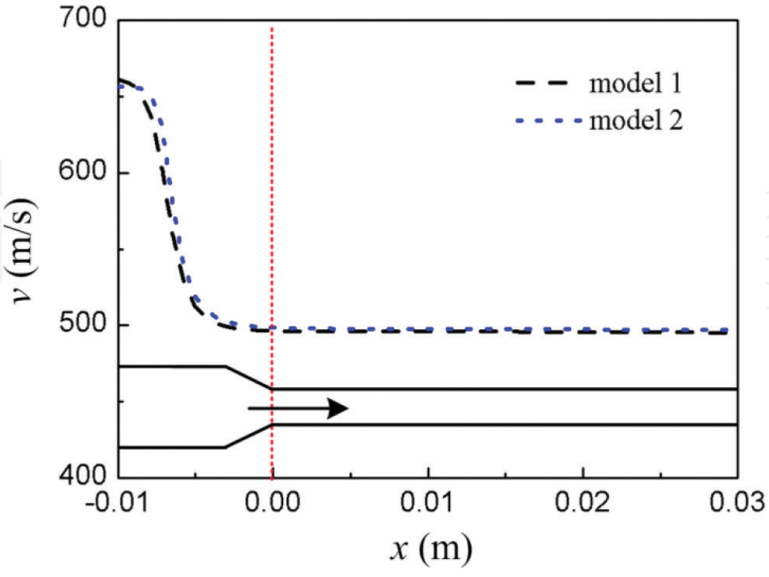

Figure 8. Velocity distributions in the axial lines of the two nozzles.

3.2. Independence analysis of particle number

As the abrasive particle concentrations on the volume fraction basis are less than 1% in the present simulations, the one-way coupling method is utilized to predict the particle trajectories, and the effects of particle movements on the continuous phases are not considered. Thus, the integration of particle paths is a post-process, which is performed after the fluid field is obtained. Since the effect of turbulent velocity on the particle paths has been accounted, the independence analysis of particle number should be conducted in order to obtain statistically representative results.

Four different particle numbers are sampled at about 60 different cross sections along the focus tube, and the results are shown in **Figure 9**. It should be noted that the particles are assumed to be spherical, and the energy loss due to particle-wall interactions is also neglected. As illustrated in **Figure 9**, the sampled particle velocities tend to collapse together with the increasing of sampled particle numbers. It is noted that when the sampled particle number is greater than 10,500, the resulted velocities do not change with further increase of sampled particles. Thus, the tracked particle number is maintained at about 10,500 in the subsequent calculations.

3.3. Effect of particle initial velocity

The particle initial velocities at the abrasive particle inlet tube are hard to determine experimentally, and thus in the abovementioned simulations, the initial velocity is set as zero uniformly, and the particles are accelerated by the entrained air phase. In order to ensure that the boundary condition for the inlet abrasive particle is reasonable, the effects of particle initial velocities on the final predicted velocities need to be further investigated. Two

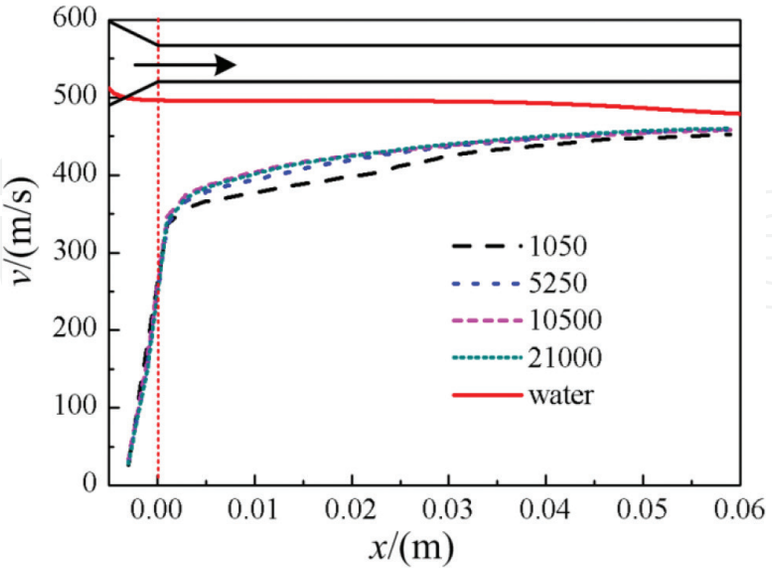

Figure 9. Velocity distribution with different particle sampling numbers (model 1).

different particle initial velocities for the two nozzles are discussed, and the sampled results are given in **Figure 10**. As it can be seen, the predicted velocities under the two different particle initial velocities coincide with each other for each model. Thus, it is confirmed that the simulated results are insensitive to the particle initial velocities within the discussed range of 0–2 m/s.

The results also indicate that the general particle accelerations for both the two AWJ nozzle models are similar. In the convergence section of the focus tubes, the particle velocities are increased linearly with the increase of the axial distance, and the velocity rises sharply from a low-level value to a high-level value. In the initial straight part of the focus tubes, the accelerations of abrasive particles are gradually weakened, and the overall velocities are approaching a constant value which is always smaller than the corresponding water speed. As the particles move further downstream in the focus tube, the velocity differences between the water and the particle are further reduced, which means that the particles are continuously accelerated by the high-speed jet flow. As shown in **Figure 10**, the velocity profiles of model 1 and model 2 have a gap in the initial section of the focus tube. The particle acceleration of model 2 is faster than that of model 1, which indicates that a larger abrasive particle inlet tube angle can enhance the particle accelerations.

3.4. Effect of shape factor

The shape factor in the drag coefficient model is introduced to account for the effects of particle shape on the drag force predictions. Two different shape factors are defined for both the two nozzle models to investigate the shape factor value on the calculated particle velocities. As given in **Figure 11**, the particle velocities under with the two different shape factors show obvious differences for both model 1 and model 2. At the convergence part of the focus tube, the corresponding two velocity curves for each nozzle model collapse together. However, at

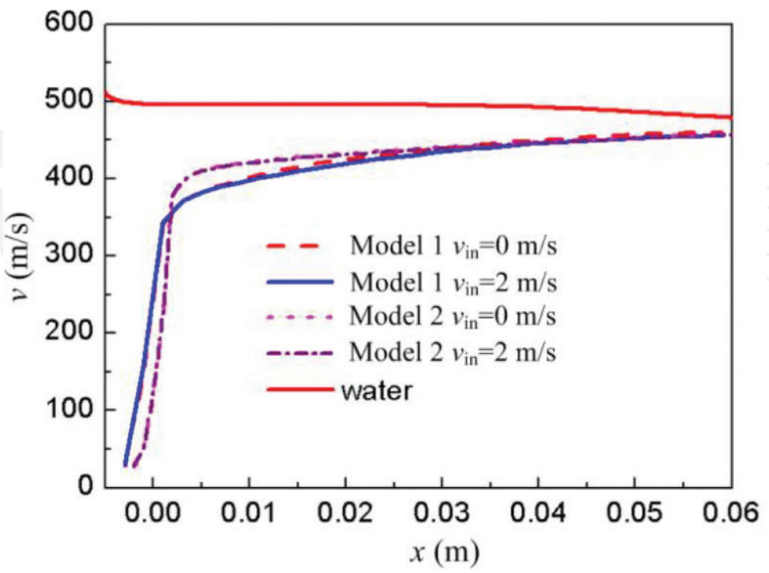

Figure 10. Velocity distributions with different particle initial velocities.

http://dx.doi.org/10.5772/intechopen.75938

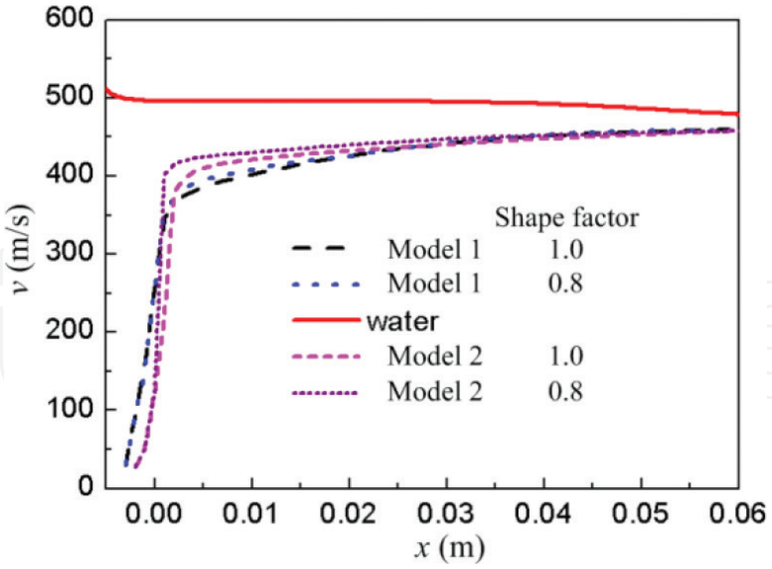

Figure 11. Velocity distributions with different shape factors.

the straight part between 0.0 and 0.04 m, the curves begin to separate, and the velocity with smaller shape factor is comparatively larger. It can be explained by the fact that the drag forces acting on the abrasive particles are larger at a smaller shape factor and thus the particles are accelerated much more quickly. At the following part, the curves again come together indicating that the particle velocities under the selected shaper factors are the same at the focus tube outlet. Thus, the results further reveal that the length of focus tube has an impact on the final particle velocities and a properly designed focus tube should be introduced to ensure that the abrasive particles are fully accelerated.

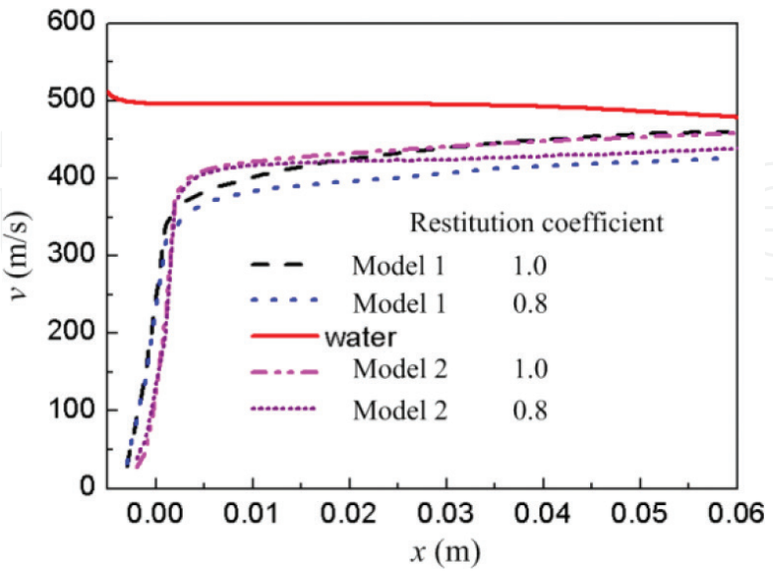

Figure 12. Velocity distributions with different restitution coefficients.

3.5. Effect of particle-wall restitution coefficient

The effects of restitution model accounting for the particle-wall interactions on the predicted velocities are studied to obtain an accurate prediction on the particle paths. When the restitution coefficients at normal and tangential directions are both set as unity, the particle energy loss upon collision is neglected. In real cases, the rebound velocity is lower than the incident velocity. In this work, two kinds of restitution coefficients for both the two AWJ nozzle models are adopted, and the predicted results are shown in **Figure 12**. With the decreased restitution coefficients, the sampled particle velocities at the straight section of the focus tube are lower for both the two models, which indicate that a proper rebound model should be introduced in order to consider the real behaviors of particle-wall interactions.

4. Conclusions

The multiphase flows inside the two AWJ nozzle models with different abrasive inlet tube angles at the same operating pressure are simulated using the standard k-ε turbulence model coupled with the VOF multiphase model based on the Euler-Lagrangian approach. The results indicate that sufficient particles should be sampled in order to obtain a statistically representative result. At the studied velocity range, the particle initial velocities for the two AWJ nozzles do not influence the predicted results. Further analysis shows that for both the two nozzles smaller particle shape factors enhance the process of particle accelerations and a proper length of the focus tube can guarantee that the particles will be fully accelerated. The restitution coefficients may have a significant influence on the particle paths as well as the predicted particle velocities. And, a proper rebound model should be introduced in order to capture the real particle behaviors in the AWJ nozzle. The abrasive inlet tube angle has little impact on the water-phase flows, while a larger abrasive inlet tube angle can enhance the particle accelerations.

Acknowledgements

This work was financially supported by the National High-Technology Research and Development Program 863 (2015AA043401).

Author details

Xinping Long[1]* and Qi Liu[2]

*Address all correspondence to: xplong@whu.edu.cn

1 School of Power and Mechanical Engineering, Wuhan University, Wuhan, Hubei, China

2 China Ship Development and Design Center, Wuhan, China

References

[1] Matsumura T, Muramatsu T, Fueki S. Abrasive water jet machining of glass with stagnation effect. CIRP Annals – Manufacturing Technology. 2011;**60**:355-358

[2] Wang J, Shanmugam DK. Cutting meat with bone using an ultrahigh pressure abrasive waterjet. Meat Science. 2009;**81**:671-677

[3] Henning A, Liu HT, Olsen C. Economic and technical efficiency of high performance abrasive waterjet cutting. Journal of Pressure Vessel Technology. 2012;**134**:021405-021405

[4] Haghbin N, Ahmadzadeh F, Spelt JK, Papini M. Effect of entrained air in abrasive water jet micro-machining: Reduction of channel width and waviness using slurry entrainment. Wear. 2015;**344-345**:99-109

[5] Axinte DA, Srinivasu DS, Kong MC, Butler-Smith PW. Abrasive waterjet cutting of polycrystalline diamond: A preliminary investigation. International Journal of Machine Tools and Manufacture. 2009;**49**:797-803

[6] Long X, Ruan X, Liu Q, Chen Z, Xue S, Wu Z. Numerical investigation on the internal flow and the particle movement in the abrasive waterjet nozzle. Powder Technology. 2017;**314**:635-640

[7] Momber AW. Energy transfer during the mixing of air and solid particles into a high-speed waterjet: An impact-force study. Experimental Thermal and Fluid Science. 2001; **25**:31-41

[8] Liu H, Wang J, Kelson N, Brown RJ. A study of abrasive waterjet characteristics by CFD simulation. Journal of Materials Processing Technology. 2004;**153-154**:488-493

[9] Lee J-H, Park K-S, Kang MC, Kang BS, Shin BS. Experiments and computer simulation analysis of impact behaviors of micro-sized abrasive in waterjet cutting of thin multiple layered materials. Transactions of Nonferrous Metals Society of China. 2012; **22**(3):s864-s869

[10] Shanmugam DK, Masood SH. An investigation on kerf characteristics in abrasive waterjet cutting of layered composites. Journal of Materials Processing Technology. 2009;**209**:3887-3893

[11] Coray PS, Jurisevic B, Junkar M, Heiniger KC. Measurements on 5:1 scale abrasive water jet cutting head models, In: Proceedings of the 6th International Conference on Management of Innovative Technologies MIT 2003 – post-conference edition. Ljubljana: University of Ljubljana; 2003. pp. 87-102

[12] Yang M, Wang Y, Kang C, Feng YU. Multiphase flow and wear in the cutting head of ultra-high pressure abrasive water jet. Chinese Journal of Mechanical Engineering. 2009;**22**:729-734

[13] Basha AT, Annoni M, Monno M, et al. Investigation of the hydrodynamic characteristics of abrasive water jet cutting head[J]. International Journal of Machining & Machinability of Materials. 2013;**14**(1):105-122

[14] Tazibt A, Parsy F, Abriak N. Theoretical analysis of the particle acceleration process in abrasive water jet cutting. Computational Materials Science. 1996;**5**:243-254

[15] Ahmed SE, Naser J, et al. Numerical Simulation of Abrasive Water Jet for Different Taper Inlet Angles, [C]//14th Australasian Fluid Mechanics Conference, Australia. 2001:645-648

[16] Haider A, Levenspiel O. Drag coefficient and terminal velocity of spherical and non-spherical particles. Powder Technology. 1989;**58**:63-70

[17] Momber AW, Kovacevic R. Principles of Abrasive Water Jet Machining. London: Springer; 1998